



# 1 Time-varying drainage basin development and erosion on 2 volcanic edifices

3 Daniel O'Hara<sup>1</sup>, Liran Goren<sup>2</sup>, Roos M.J. van Wees<sup>1</sup>, Benjamin Campforts<sup>3</sup>, Pablo Grosse<sup>4,5</sup>,  
4 Pierre Lahitte<sup>6</sup>, Gabor Kereszturi<sup>7</sup>, Matthieu Kervyn<sup>1</sup>

5 <sup>1</sup>Department of Geography, Vrije Universiteit Brussel, Pleinlaan 2, 1050 Elsene.

6 <sup>2</sup>Ben Gurion University of the Negev, Department of Earth and Environmental Sciences, Beer-Sheva, Israel

7 <sup>3</sup>Institute of Arctic and Alpine Research, University of Colorado Boulder, Boulder, CO, USA

8 <sup>4</sup>Consejo Nacional de Investigaciones Científicas y Técnicas (CONICET), Argentina

9 <sup>5</sup>Fundación Miguel Lillo, Miguel Lillo 251, (4000) Tucumán, Argentina

10 <sup>6</sup>Université Paris-Saclay, CNRS, Laboratoire GEOPS, Rue du Belvédère, 91405 Orsay, France

11 <sup>7</sup>Volcanic Risk Solutions, School of Agriculture and Environment, Massey University, 4474, New Zealand

12 *Correspondence to:* Daniel O'Hara (Daniel.OHara@vub.be)

13 **Abstract.** The erosional state of a landscape is often assessed through a series of metrics that quantify the  
14 morphology of drainage basins and divides. Such metrics have been well-explored in tectonically-active  
15 environments to evaluate the role of different processes in sculpting topography, yet relatively few works have  
16 applied these analyses to radial landforms such as volcanoes. We quantify drainage basin geometries on volcanic  
17 edifices of varying ages using common metrics (e.g., Hack's Law, drainage density, number of basins that reach the  
18 edifice summit, as well as basin hypsometry integral, length, width, relief, and average topographic slope). Relating  
19 these measurements to the log-mean age of activity for each edifice, we find that drainage density, basin  
20 hypsometry, basin length, and basin width quantify the degree of erosional maturity for these landforms. We also  
21 explore edifice drainage basin growth and competition by conducting a divide mobility analysis on the volcanoes,  
22 finding that young volcanoes are characterized by nearly-uniform basin geometries in unstable configurations that  
23 are prone to divide migration. Finally, we analyze basin spatial geometries and outlet spacing on edifices,  
24 discovering an evolution in radial basin configurations that differ from typical linear mountain ranges. From these,  
25 we present a novel conceptual model for edifice degradation that allows new interpretations of composite volcano  
26 histories and provides predictive quantities for edifice morphologic evolution.

## 27 1.0 Introduction

28 Understanding how drainage basins on eroding landforms develop and evolve is a fundamental principle of  
29 Geomorphology. Over regional scales, basin geometry, structure, and spacing evolve in response to both external  
30 (e.g., climate, tectonics; Castelltort et al., 2012; Duvall and Tucker, 2015; Han et al., 2015; Yang et al., 2015) and  
31 internal (e.g., channel piracy; Bishop, 1995; Whipple et al., 2016) forcing as topographic slopes adjust to develop  
32 and maintain an equilibrium between erosion and uplift (e.g., Willett et al., 2001; Castelltort et al., 2009). As these  
33 landscapes adjust, transient signals within basins propagate upstream to surrounding channel heads, where opposing  
34 signals between adjacent basins drive divide migration that modify available area for overland flow (e.g., Willett et  
35 al., 2014; O'Hara et al., 2019).

36 Work in the 20<sup>th</sup> century established foundational relationships between basin drainage areas, lengths, and slopes  
37 (e.g., Horton, 1945; Strahler, 1952; Hack, 1957; Flint, 1974), providing the basis for analyzing landscape  
38 disequilibrium and evolution in both tectonically-active (e.g., Kirby and Whipple, 2012; Fox et al., 2014) and  
39 passive regions (Prince and Spotila, 2013; Willett et al., 2014; Braun, 2018). These relationships are built on the  
40 assumption of a dominantly-dendritic fluvial network existing on a near-linear primary landform (e.g., a mountain  
41 range; Castelltort and Simpson, 2006). Furthermore, basin competition is often considered in the simplified

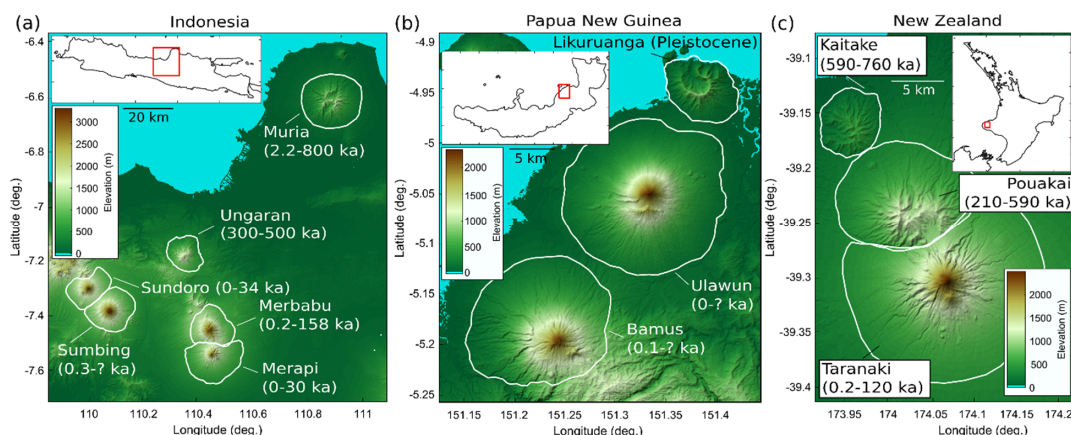


42 configuration of a binary drainage system, where a divide supports only two opposing basins that compete across it  
43 (e.g., Gilbert, 1909; Mudd and Furbish, 2007).

44 Although dendritic channel networks are most prevalent on Earth, they are not the only type of configuration.  
45 Trellis, rectangular, parallel, and radial drainages also occur (Howard, 1967). The formation of these other drainages  
46 often relate to the region's tectonic, volcanic, or glacial history, subsurface structure, or geometry of the primary  
47 landform that they erode (Zernitz, 1932). However, compared to dendritic basins, studies that explore the geometries  
48 and evolution of other drainage settings are scarce (e.g., Mejía and Niemann, 2008; Becerril et al., 2021; Hamawi et  
49 al., 2022).

50 Volcanic edifices are characterized by radial drainages. In these settings, quantifying drainage evolution can be  
51 challenging as these landforms experience interspersed, short-term eruptive episodes superimposed onto the long-  
52 term degradation record (e.g., Thouret et al., 2014). Additionally, drainage formation can lag behind surfacing by  
53 volcanic deposits over 1 – 100 kyr timescales due to transmission losses associated with permeable volcanic  
54 material (e.g., lava flows, pyroclasts; Lohse and Dietrich, 2005; Jefferson et al., 2010; Sweeney and Roering, 2017).  
55 Finally, the binary drainage divide typical of linear mountain ranges breaks down on volcanic edifices due to their  
56 radial nature, with multiple catchments constrained to the conical structure of the volcano and converging towards a  
57 single main summit. Despite these challenges, volcanic edifices represent ideal primary landforms to investigate  
58 drainage evolution due to their well-defined conical initial conditions, datable surfaces, and scarce inheritance from  
59 regional tectonics. Furthermore, quantifying the relationships between edifice construction and drainage basin  
60 morphology provides new insight for investigating edifices remotely, and can thus expand our understanding of  
61 basin dynamics while also complimenting field-based surveys to resolve volcano edifice histories.

62 Here, we explore the development of drainage basins and topography on stratovolcanoes from Indonesia, Papua  
63 New Guinea, and New Zealand (Fig. 1). Using common hydrographic metrics and broad volcanic histories, we  
64 determine stages of maturation during basin evolution and derive a new generalized model for volcanic edifice  
65 degradation that builds off of previous studies (Ollier, 1988). We then quantify divide mobility on radial structures  
66 within the context of our conceptual model and discuss the applicability of our analyses to characterize an edifice's  
67 history.



68

69 **Figure 1 – Regional maps of 12 analyzed edifices from (a) Indonesia, (b) Papua New Guinea, and (c) New Zealand. White**  
70 **lines represent edifice boundaries. Text describes volcano names and known ages of activity (Table T2).**

## 71 **2.0 Methods**

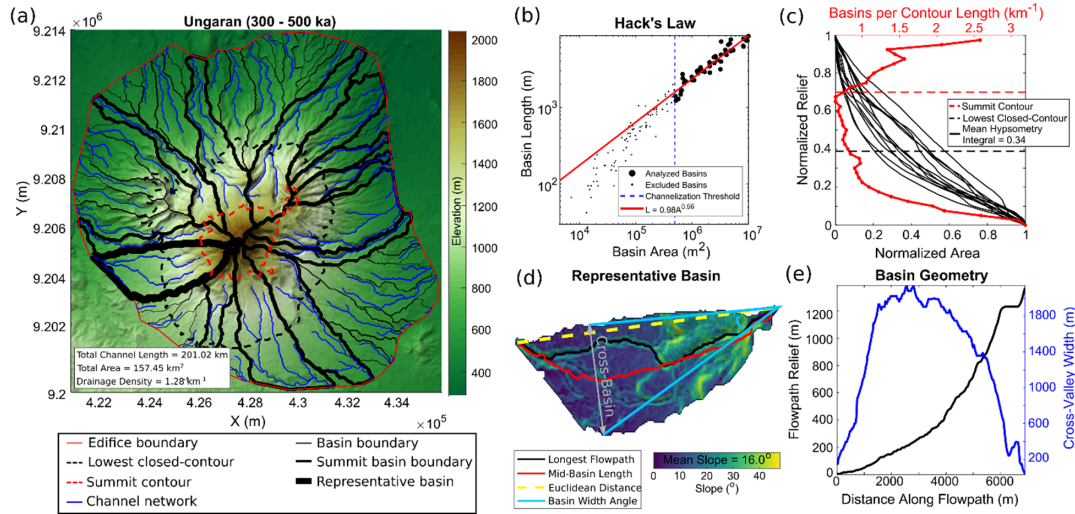
72 We focus on closely-spaced sets of volcanic edifices (Fig. 1). Within each respective region, volcano sets are fed by  
73 similar magma sources and likely experienced similar climate conditions, but the volcanoes were active over  
74 different time intervals and show spatially-varying degrees of degradation. We exclude complex massifs from the  
75 analysis and consider only relatively simple edifices.

### 76 **2.1 Edifice Delineation**

77 We follow the method of van Wees et al. (2021) to delineate edifice boundaries from surrounding topography.  
78 Although automated algorithms exist to generate boundaries (e.g., Bohnenstiehl et al., 2012; Euillades et al., 2013),  
79 these often create conservative limits around the edifice that ignore lower flanks and volcano-sedimentary aprons  
80 (e.g., O’Hara et al., 2020). Using 30-m Shuttle Radar Topography Mission (SRTM) Digital Elevation Models  
81 (DEMs) (Farr et al., 2007), we first generate hillshade, aspect, and slope angle rasters of the raw topography. Lower  
82 edifice flanks are generally characterized by slope angles greater than some threshold value (Karátson et al., 2012);  
83 we therefore filter topography using a 300 m wavelength and reclassify the slope map using a 3° slope threshold  
84 (van Wees et al., 2021). Using these maps as visual aids, we then hand-draw boundaries that separate the edifice  
85 from surrounding terrain. Afterwards, the DEMs are clipped using these boundaries to isolate the edifices for  
86 morphometric analysis. None of the chosen volcanoes have closed summit craters, recognizable collapse scars, or  
87 any other irregular surface that required special preprocessing; we thus use the entire edifice topography for our  
88 analysis.

### 89 **2.2 Edifice Basin Morphology**

90 We analyze edifice basin morphologies with DrainageVolc, a series of scripts modified from TopoToolbox  
91 (Schwanghart and Scherler, 2014), which is designed to investigate volcanic topography through a set of  
92 topography-, drainage-, and channel-based analyses. The metrics considered here are commonly used within  
93 tectonic settings but have not previously been applied to radial drainages. Figure 2 displays an example of our  
94 methods using the Ungaran volcano in Indonesia.



95

96 **Figure 2 – Analyzed basin metrics. a: Map of Ungaran volcano (Indonesia), colored lines defined in legend. b: Hack's**  
 97 **Law relationship between basin areas and lengths. Black circles are basins used in power-law analysis, black dots are**  
 98 **excluded basins; blue-dashed line is drainage area threshold ( $A_T$ ;  $0.5 \text{ km}^2$ ) for channelization. c: Scaled edifice metrics.**  
 99 **Red line shows normalized number of basins along elevation contours. Black lines are summit basin hypsometry curves.**  
 100 **d: Local slope and geometry values of representative basin (thick black line in 2a). Gray line represents cross-basin**  
 101 **direction perpendicular to the Euclidean basin length. e: Cross-basin values along basin shown in 2d. Black line is relief**  
 102 **along flowpath, blue line is cross-valley width.**

103 We first fill sinks in the DEM through TopoToolbox's preprocessing algorithm (Schwanghart and Scherler, 2014) to  
 104 ensure continuous flow to the edifice boundary and extract drainage basins from topography using steepest-descent  
 105 flow routing (Fig. 2a). We then perform a series of analyzes related to basin geometry. The lengths ( $L$ ) of all basins  
 106 draining to the edifice boundaries are calculated by determining mid-point paths between basin divides  
 107 perpendicular to the Euclidean distance between the highest and lowest reaches of the basin, irrespective of whether  
 108 there is an actual flow channel in this path (Fig. 2d). Assuming basins with drainage areas ( $A$ ) greater than some  
 109 threshold ( $A_T$ ) support overland flow, we then explore the correlation between the lengths and drainage areas of  
 110 these basins through a power-law regression to derive the Hack's Law relationship (Fig. 2b) for the edifice as (Hack,  
 111 1957)

$$112 \quad L = k_a A^H, \tag{1}$$

113 where  $k_a$  and  $H$  are Hack's coefficient and exponent, respectively.  $H$  values are compared across edifices as this  
 114 exponent describes general basin geometry, with values of  $\sim 0.47 - 0.6$  typically attributed to dendritic systems  
 115 (Hack, 1957; Mueller, 1972). Our Hack's Law derivation uses mid-point basin lengths as opposed to typical flow  
 116 path lengths to remove the effects of channel sinuosity and focus explicitly on basin geometry; however, within the  
 117 context of our edifice basins, this derivation does not significantly alter our results, and values are thus comparable  
 118 to those of previous studies (Fig. S1). We also analyze the density of the edifice's channel network by extracting



119 flow paths with drainage areas greater than  $A_T$  from the landform, and calculate the edifice-scale drainage density as  
120 (Horton, 1945)

$$121 \quad DD = \frac{\sum L_c}{A_E}, \quad (2)$$

122 where  $\sum L_c$  is the cumulative sum of all channel lengths and  $A_E$  is the planform area of the edifice's boundary (Fig.  
123 2a). Using an automated slope-area analysis of basins to determine the drainage area threshold that best corresponds  
124 with the power-law decrease in slope (Montgomery and Dietrich, 1994) for each edifice, we find  $A_T$  ranges between  
125  $0.32 - 1.42 \text{ km}^2$ , with a mean threshold of  $0.78 \text{ km}^2$  (Supplemental text). For consistency across all edifices, we  
126 assume a constant drainage area threshold of  $0.5 \text{ km}^2$  to delineate networks. Sensitivity analysis (Fig. S3)  
127 demonstrates that although the selection of  $A_T$  does not significantly impact the general behavior of drainage density  
128 results, the Hack's Law exponent is more sensitive to this choice.

129 Afterwards, we calculate mean values of basin geometries on each edifice. Rather than analyze the geometry of all  
130 basins that exist on a volcano, we limit our analysis to larger basins that best characterize the edifice's drainage, and  
131 thus its dismantling. These large characteristic basins may be determined using a variety of methods, such as  
132 through an arbitrary number or percentage of basin sizes, using the basins that are within some radial distance of the  
133 edifice's peak, or determining basins that extend to some portion of the edifice's height. Determining characteristic  
134 basins by an arbitrary number or percentage of basin sizes may introduce bias as the population of basins drastically  
135 vary between edifices (Fig. 8a), whereas determining characteristic basins by radial distance from the edifice's peak  
136 introduces geometric constraints as edifice shapes often deviate from the textbook symmetric, single-peaked edifice,  
137 instead developing large, irregular summit regions that are defined by high topography and multiple peaks (e.g.,  
138 Karátson et al., 1999; Grosse et al., 2012). As slope (and thus elevation) is an essential component of erosion and  
139 basin development (Hack, 1957; Flint, 1974), we define characteristic basins as those that reach the edifice's summit  
140 region. However, we note that defining characteristic basins based on radial distance can produce different trends  
141 (Fig. S4), and may be more appropriate for some of our analyzed metrics (Section 5.3).

142 Generating a series of elevation contours along the edifice at intervals of 2.5% of the edifice's relief, we calculate  
143 the number of basins that intersect each contour, normalized by the contour's length (Fig. 2c, red line). For all  
144 edifices, we define the edifice's summit as the upper 30% of the edifice's relief, and thus consider the basins that  
145 reach this summit region (referred here as *summit basins*) as those that best characterize the edifice's drainage  
146 development. We then determine summit basin numbers, mean basin slopes (Fig. 2d), basin lengths ( $L_B$ ; Fig. 2d, red  
147 line), basin reliefs (Fig. 2e, black line), and maximum cross-basin widths ( $W_B$ ; Fig. 2e, blue line). To compare  
148 values across edifices of varying sizes, summit basin numbers are normalized by the length of the summit contour  
149 (Fig. 2c) and basin reliefs are normalized by the relief of the entire edifice. We also utilize the radial nature of  
150 edifices to generate normalized values of basin length ( $L'_B$ ) and width ( $W'_B$ ) as

$$151 \quad L'_B = \frac{L_B}{L_E}, \quad (3)$$



152 and

$$153 \quad W'_B = 2 \tan^{-1} \left( \frac{W_B/2}{L_{WB}} \right), \quad (4)$$

154 respectively, where  $L_E$  is the edifice's effective radius, defined as the radius of the circle with the same planform  
155 area ( $A_E$ ) as the edifice's boundary ( $L_E = \sqrt{A_E / \pi}$ ), and  $L_{WB}$  is the distance from the highest point within a basin to  
156 where the basin is widest.  $W'_B$  thus converts basin widths into an angle relative to the summit (Fig. 2d, light blue  
157 lines). Mean values of these quantities are then calculated for each edifice.

158 We also calculate mean summit basin hypsometry integrals for each edifice (Strahler, 1952; Fig. 2c, black lines).  
159 Individual basin hypsometry curves ( $H_C$ ) are derived by counting the number of basin pixels  $N_{PB}$  at or above  
160 normalized elevation values ( $Z$ , ranging from 0 to 1); afterwards, these values are normalized by the total number of  
161 basin pixels ( $N_{PTot}$ ) as

$$162 \quad H_C(Z_I) = \frac{N_{PB}(Z \geq Z_I)}{N_{PTot}}, \quad (5)$$

163 where  $I$  is a counter over normalized elevation values from 0 to 1. Hypsometry integrals of each basin are calculated  
164 as the positive integration over the curves from eq. (5). These are also averaged for each edifice.

### 165 **2.3 Edifice Landform Morphology**

166 As well as studying the temporal evolution of drainages on edifices, we also consider the broad geometry of the  
167 volcanoes. Grosse et al. (2009, 2012) developed the initial MorVolc algorithm in IDL, which quantifies edifice  
168 morphologies through a series of size, shape, slope, orientation, peak, and summit parameters. Using the same  
169 framework as DrainageVolc, we redeveloped the IDL code in Matlab, also utilizing the TopoToolbox DEM analysis  
170 package (Schwanghart and Scherler, 2014). Both DrainageVolc and the updated MorVolc scripts are available for  
171 use on GitHub ([https://github.com/danjohara/Volc\\_Packages](https://github.com/danjohara/Volc_Packages)).

172 We analyze simple edifice geometry measurements with this updated version of MorVolc, including effective  
173 radius, height, height-radius ratio, and mean slope of the main flank (edifice region between the lowest closed-  
174 contour that encompasses the edifice and the edifice's summit contour). We also quantify the mean contour  
175 ellipticity and irregularity indices of the main flank from the previously-computed contours. The ellipticity index  
176 ( $EI$ ) describes the elliptical nature of the edifice elevation contours, and is defined as

$$177 \quad EI = \frac{\pi(L_M/2)^2}{A_C}, \quad (6)$$



178 where  $L_M$  is the length of the major axis of a best-fitting ellipse through the contour and  $A_C$  is the area enclosed by  
179 the contour (Grosse et al., 2012). The irregularity index ( $II$ ) describes divergence of the contour from a smooth  
180 ellipse as

$$181 \quad II = di_{contour}(di_{ellipse} - 1), \quad (7)$$

182 where  $di$  is the dissection index, defined as

$$183 \quad di = \frac{P_C}{2A_C} \sqrt{A_C/\pi}, \quad (8)$$

184 with  $P_C$  and  $A_C$  being the perimeter and area of the contour, respectively (Grosse et al., 2012). Finally, we also  
185 incorporate new measurements within MorVolc, including the slope variance of the entire edifice (standard  
186 deviation of all slope values divided by the mean slope, similar to roughness), as well as a minimum eroded volume  
187 estimate. Eroded volume is estimated from a convex-hull reconstruction of the edifice, using the methodology  
188 described in O'Hara and Karlstrom (2023). Afterwards, eroded volume is normalized as a percent relative to the  
189 total reconstructed volume.

## 190 **2.4 Edifice Ages**

191 To explore morphological evolution through time, we correlate edifice landform and drainage basin metrics to  
192 volcano ages of activity. We thus compile known eruption records of each volcano, with ages ranging from present  
193 to early Pleistocene (Table T2). Volcanoes often have complex surface evolutions, with lifespans of activity that  
194 range 100-1000 kyrs and characterized by stochastic episodes of growth interspersed with periods of erosion during  
195 quiescence (e.g., Karátson et al., 1999; Lahitte et al., 2012). Furthermore, episodes of activity are often constrained  
196 to localized regions of the edifice and thus do not fully resurface the entire landform (e.g., Civico et al., 2022).  
197 Similarly, erosion across the edifice is typically non-uniform as local conditions are dependent on the age and type  
198 of activity within the vicinity (e.g., Ferrier et al., 2013; Pierson and Major, 2014; Thouret et al., 2014; Ricci et al.,  
199 2015).

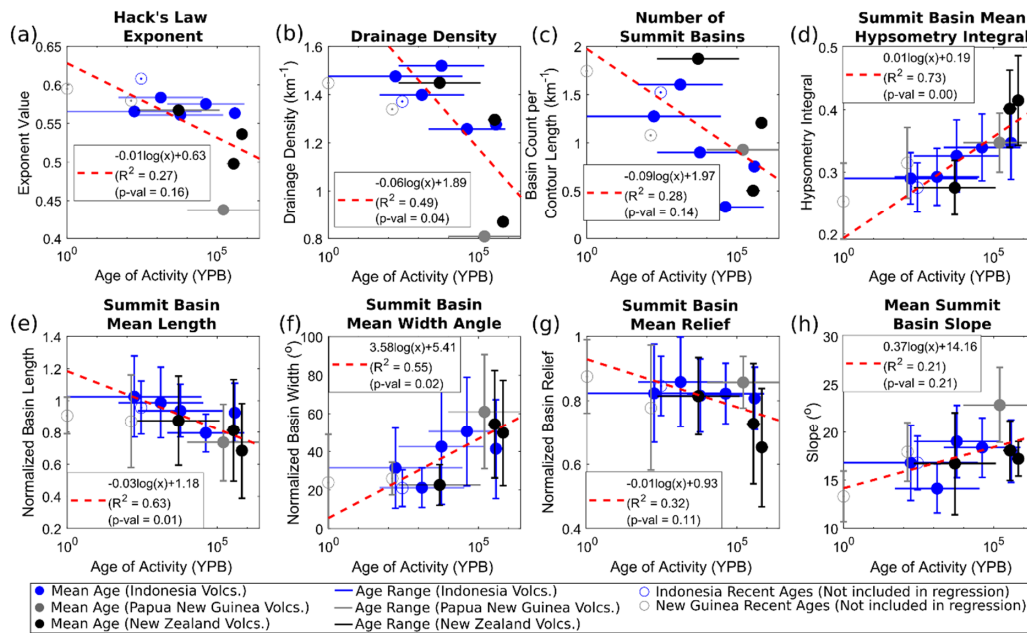
200 Despite the spatial and temporal heterogeneities of activity and erosion, we argue that a generalized morphologic  
201 age of an edifice may be derived that quantifies the erosional state of the landform and relates to the edifice's  
202 lithologic age. To account for the time differences between short-term events and the cumulative long-term history  
203 on morphology, we define an edifice's age as a single value using the log-mean between the most recent eruption  
204 and oldest date of activity. This definition thus accounts for the span of temporal magnitudes; however, we note that  
205 using linear-mean ages produce similar results (Fig. S5). Afterwards, we analyze the temporal evolution of edifice  
206 morphologies by fitting logarithmic relationships between edifice age and morphometric parameters. Some  
207 volcanoes (Sumbing, Bamus, and Ulawun) have poorly-documented histories (only the most recent eruption has  
208 been dated) and are therefore excluded from the regression. Conversely, Likuruanga is only known to have erupted  
209 during the Pleistocene and is incorporated in the analysis.



210 **3.0 Results**

211 We find trends between volcano age and our morphometric metrics through time (Figs. 3-4; Supplemental Table  
 212 T3). Considering all metrics, we find that edifice height, effective edifice radius, mean irregularity index (with the  
 213 exception of an outlier; Fig. 4e), mean ellipticity index, edifice slope variance, normalized eroded volume, drainage  
 214 density, mean summit basin hypsometry integral, normalized basin length, and normalized basin width have  $R^2$   
 215 values ranging 0.38 – 0.75 and correlation p-values  $< 0.1$ , suggesting these metrics provide quantitative measures to  
 216 characterize the overall maturity of the edifice. Other metrics have weaker correlation values (0.21 – 0.32) and are  
 217 statistically insignificant (with p-values of 0.11 – 0.21), and thus may be more sensitive to the initial edifice  
 218 geometry or other processes that alter edifice morphology, or that age is not a significant factor for these metrics.  
 219 The noted outlier in irregularity index is Muria (Indonesia) and originates from two broad fluvial networks on  
 220 opposite flanks that are deeply incised into the landform and may be associated with breached craters (Fig. 1a).

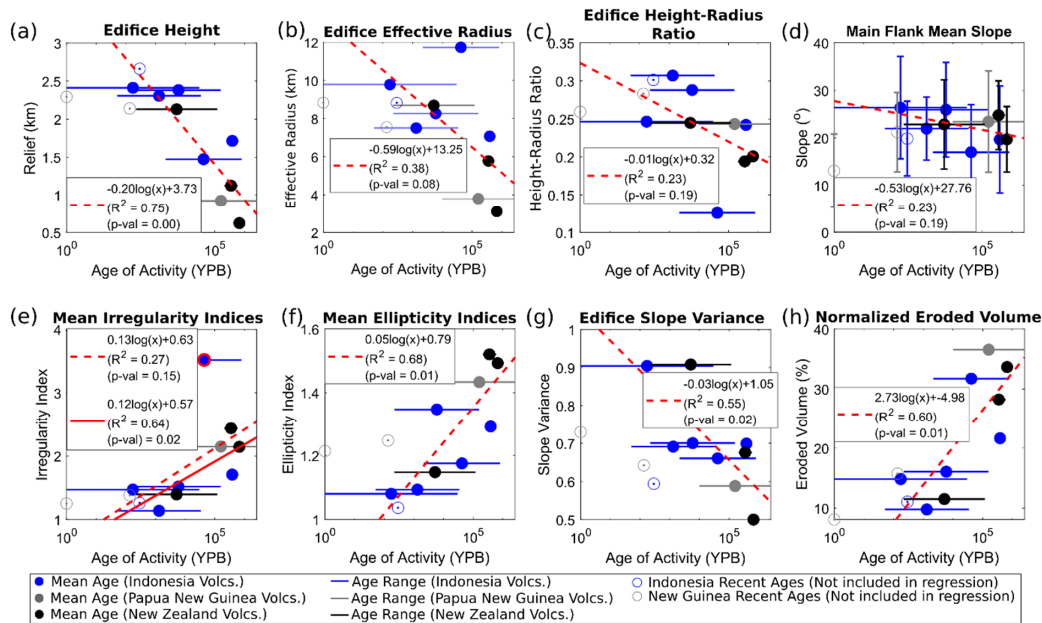
221 Of the statistically-significant metrics related to edifice drainage morphology, mean summit basin hypsometry  
 222 integral and normalized width increase through time, whereas drainage density and mean summit basin normalized  
 223 length decrease (Fig. 3). Similarly, considering statistically-significant metrics related to the edifice as a primary  
 224 landform, mean irregularity index, mean ellipticity index, and convex-hull based eroded volumes increase with age,  
 225 while edifice height, effective radius, and slope variance decrease with age (Fig. 4).



226

227 **Figure 3 – Temporal relationships of drainage basin morphology metrics.** Colors correspond to volcanic region.  
 228 Horizontal lines are edifice age ranges of activity, with filled circles representing log-mean age. Vertical lines represent  
 229 one standard deviation of values (where appropriate). Red-dashed lines and equations characterize logarithmic  
 230 regressions; open circles are excluded in the regression due to age limitations.





231

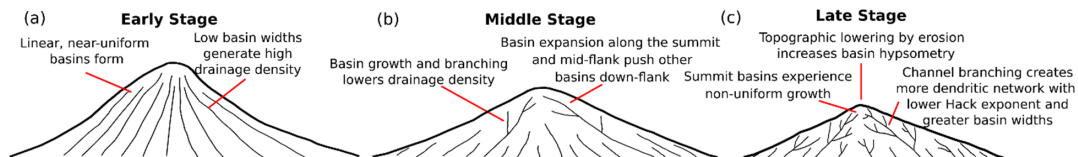
232 **Figure 4 – Temporal relationships of landform morphology metrics. Colors and symbols are same as those described in**  
 233 **Fig. 3. Solid red line in e is secondary regression with Muria (red circle) excluded.**

234 **4.0 Discussion**

235 **4.1 Generalized model for edifice degradation**

236 The evolution of volcanic edifices as primary landforms and the drainage basins that erode them are inextricably  
 237 linked. Our results thus establish a new framework for evaluating volcanic edifices by considering both the landform  
 238 and its drainage systems. This evolutionary model expands on stages previously defined qualitatively (Ollier, 1988)  
 239 and follows similar evolution to drainages observed in badlands (Schumm, 1956).

240 Erosion of a volcanic edifice can be described within the context of our metrics by considering a simplified, conical  
 241 edifice (Fig. 5). In the initial stages of erosion (~10% of eroded volume; Fig. 5a), narrow (~20° normalized width  
 242 angle) and uniform (normalized mean length near 1) drainages form that extend from the summit region to the lower  
 243 flanks (i.e., ‘parasol ribbing’; Ollier, 1988), giving a high drainage density (~1.5 km<sup>-1</sup>).



244

245 **Figure 5 – Conceptual model of edifice dissection based on analysis results. Thin black lines represent drainage systems.**

246



247 As the edifice degrades to 30-40% eroded volume on 10-100 kyr timescales (Fig. 5b-c), both its height and area  
248 decrease; however, height decreases faster, leading to a decrease in height-radius ratios. The erosion of the edifice is  
249 accompanied by drainage basin growth, with summit basins expanding azimuthally along the edifice to normalized  
250 basin widths of 40-60°, pushing the headwaters of other basins down the edifice flanks. Furthermore, as summit  
251 basins expand, they incise into the edifice flanks and develop a more dendritic structure associated with lower  
252 drainage density ( $\sim 1 \text{ km}^{-1}$ ). This is accompanied by non-uniform summit basin lengthening; combined with possible  
253 volcanic activity that can influence landform asymmetry (i.e., causing a higher ellipticity index), non-uniform basin  
254 growth causes normalized basin lengths to decrease below 1.

255 As the edifice erodes, processes occur over varying scales to alter general edifice morphology: 1) over the entire  
256 edifice, erosion-driven topographic lowering occurs faster than horizontal areal loss of the edifice, creating a flatter  
257 landform; and 2) at the scale of a basin, incision carves into the initially-planar flanks of the edifice, steepening  
258 surrounding valley walls and increasing contour irregularity. The relationship between basin-scale incision and  
259 edifice-scale flattening is recorded through summit basin hypsometry integrals and the slope variance of the entire  
260 edifice. The decrease in edifice slope variance suggests mean edifice slopes increase relative to the standard  
261 deviation of slope, thus suggesting overall steepening of topography. However, increasing values of summit basin  
262 hypsometry integrals suggest that edifice-scale flattening is the dominant process. This leads to a scale-dependent  
263 behavior in edifice morphology – although the edifice as a landform is becoming flatter, incision causes local relief  
264 within the bounds of the landform to become steeper.

265 This conceptual model represents a generalized view of edifice degradation, as a variety of processes (both volcanic  
266 and erosional) can impact an edifice's morphology throughout its lifespan. Furthermore, other climate conditions not  
267 considered here (e.g., glaciers, arid environments) are expected to alter the patterns and rates of basin evolution.  
268 Nonetheless, we propose that, barring major events that significantly alter topography, composite volcano  
269 degradation generally follows the model presented here.

#### 270 **4.2 How do basins compete on radial structures?**

271 Our results suggest that drainages on radial structures are highly dynamic. From initially-uniform basin geometries,  
272 preferential erosion causes basins near the summit to become more dominant and expand, forcing other basins  
273 down-flank and generating a 'topographic hierarchy', with higher-order basins spanning the entire flank of the  
274 edifice and lower-order basins occurring on lower sections, analogous to inferred basin evolution on linear fault  
275 blocks (Talling et al., 1997). This hierarchy of basin ordering is a direct product of non-uniform basin development  
276 over the edifice that contributes to the preservation of less-eroded portions of the lower flanks (i.e., planèzes; Ollier,  
277 1988).

278 Non-uniform basin development and transience is a natural component of landscape evolution (e.g., Hasbargen and  
279 Paola, 2000); however, various factors (both volcanic and non-volcanic) can influence erosional patterns and  
280 accentuate basin growth across volcanic edifices. These may include 1) local slope changes associated with  
281 magmatic intrusions (e.g., Wicks et al., 2002; Biggs et al., 2010; Castro et al., 2016) or mass-wasting (e.g., Ui and  
282 Glicken, 1986; Shea and van Wyk de Vries, 2008); 2) variable volcanic eruption activity that increase sediment

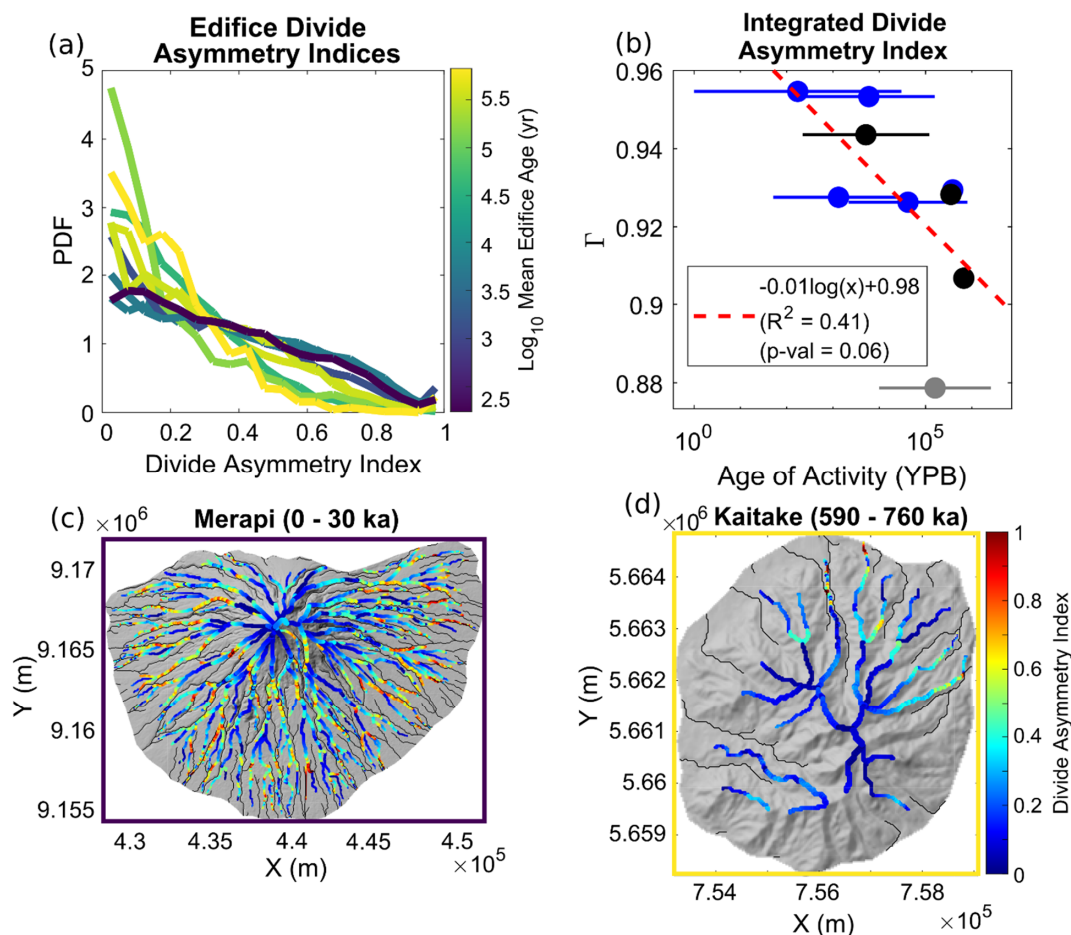


283 loads (Hayes et al., 2002; Pierson and Major, 2014), alter infiltration and rock erodibility (e.g., Wells et al., 1985;  
284 Sklar and Dietrich, 2001; Jefferson et al., 2010), or remove bedrock through scouring by pyroclasts (Gase et al.,  
285 2017) or melting by lava flows (i.e., thermal erosion; Kerr, 2001) during deposition; 3) non-uniform changes in  
286 overland flow and stream power associated with breached craters (e.g., Karátson et al., 1999) or edifice-scale  
287 precipitation gradients (e.g., Ferrier et al., 2013); and 4) downstream alterations to drainage channels that migrate  
288 upstream as a propagating incision wave (i.e., knickpoints; Kirby et al., 2003; Cook et al., 2013; Perron and Royden,  
289 2013). The long-term compilation of such processes helps drive non-uniform erosion across the edifice, which in  
290 turn encourages divide migrations and changes in basin size and geometry. More specifically, basins that exhibit  
291 higher erosion rates would tend to expand at the expense of their neighboring basins and potentially become the  
292 dominant basins, while lower erosion rates will cause other basins to shrink and their boundaries to migrate further  
293 down the edifice's flank.

294 The morphology of drainage divides is sensitive to differences in erosion between neighboring basins and can thus  
295 be used to characterize basin competition. We quantify basin geometry unsteadiness through an exploration of  
296 divide stability using the *divide asymmetry index* (*DAI*; Forte and Whipple, 2018; Scherler and Schwanghart, 2020),  
297 calculated as the positive difference in hillslope relief (vertical distance between the ridge and nearest channel)  
298 across a divide and normalized by the sum of hillslope reliefs, ranging between 0 (symmetric) and 1 (asymmetric).  
299 We limit our analysis to only consider divides that have a Strahler order greater than 1 (Scherler and Schwanghart,  
300 2020).

301 The divide mobility is expressed using probability density functions (PDFs) of *DAI* for all volcanoes (Fig. 6a). A  
302 clear temporal trend emerges – older volcanoes have distributions clustered around lower ( $< 0.4$ ) *DAI* that rapidly  
303 decrease with increasing *DAI*; while younger volcanoes show monotonically-decreasing distributions, with fewer  
304 normalized populations of low-*DAI* and greater normalized populations of high-*DAI* values compared to older  
305 volcanoes. Integrating these PDFs into single values (referred to here as  $\Gamma$ ; Fig. 6b) shows a moderate ( $R^2 = 0.41$ )  
306 correlation with age.

307 Combined with basin morphology trends (Fig. 3), this suggests younger volcanoes have basins with more uniform  
308 planform geometries and less-stable basin configurations. As the edifice erodes, basin planform geometries become  
309 less uniform, but develop more stable configurations as evidenced by the greater symmetry of hillslope relief across  
310 divides. The relationship between basin non-uniformity and stability can be observed spatially by comparing *DAI*  
311 values between Merapi (youngest) and Kaitake (oldest) volcanoes (Fig. 6c-d). Highest *DAI* values on both  
312 volcanoes generally occur at the mid- and lower-flanks of the volcano, suggesting basin expansion occurs mainly  
313 azimuthally along edifice flanks, rather than across the edifice summit. This spatial analysis highlights the process  
314 that generates topographic hierarchy – by expanding azimuthally, basin growth drives less-dominant basins down-  
315 flank through a zippering process, creating drainages with tapered geometries along the lower flanks.



316

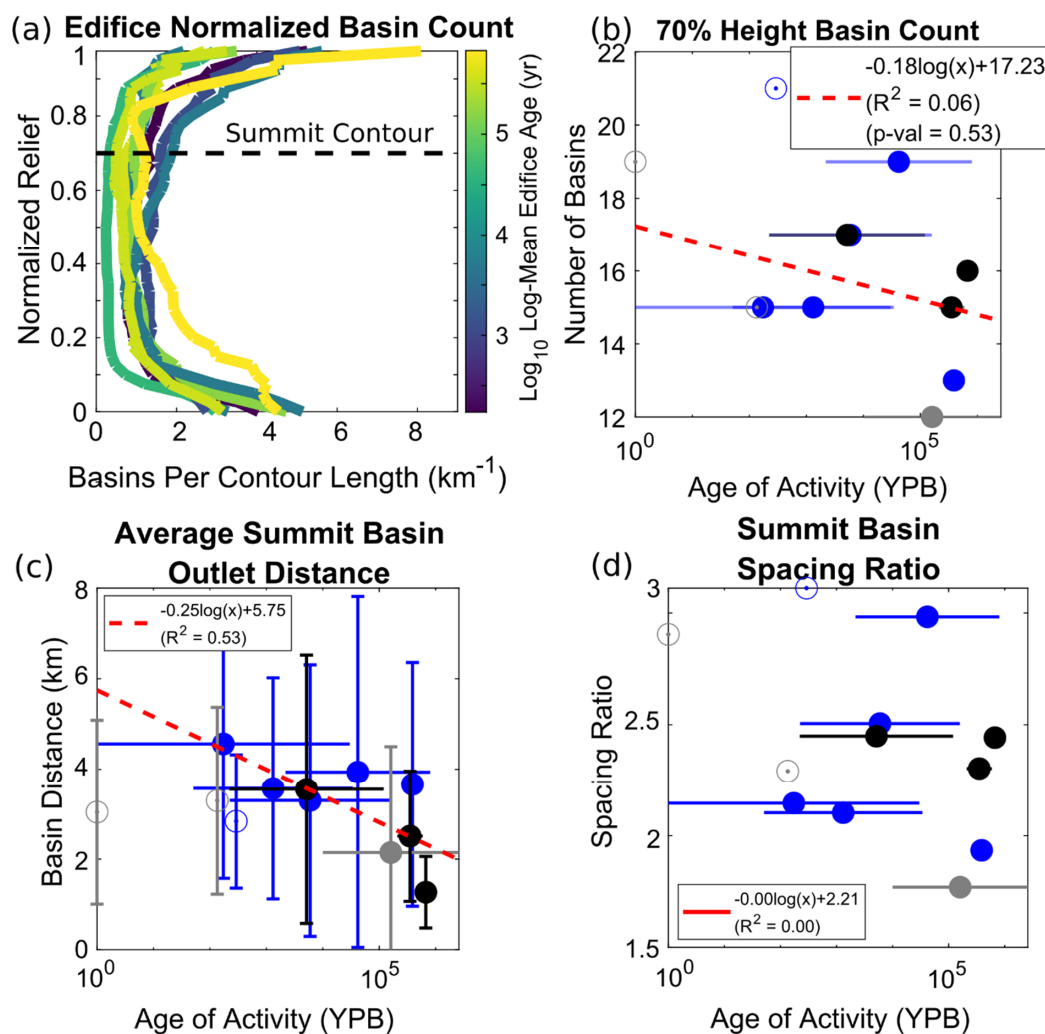
317 **Figure 6 – a:** Probability density functions (PDFs) of volcano divide asymmetry indices (DAI); colors correspond to log-  
 318 mean edifice ages. **b:** Integral of PDFs ( $\Gamma$ ) compared to edifice age. Colors and symbols are the same as Fig. 3. **c-d:** DAI  
 319 values for (c) Merapi and (d) Kaitake at the divides, black lines are edifice channel network. Border colors correspond to  
 320 ages in a.

### 321 4.3 Edifice basin widths and spacing

322 Our results show that edifices experience the same morphologic trends when considering the number of basins along  
 323 edifice relief (Fig. 7a): lower flanks are characterized by normalized basin numbers between 2–6 km<sup>-1</sup>, main flanks  
 324 are characterized by relatively consistent normalized basin numbers < 2 km<sup>-1</sup>, while the normalized basin numbers  
 325 increase near the summit (upper 30% of the edifice). This trend appears to occur largely independent of age, even  
 326 within the upper flank (as demonstrated by a low R<sup>2</sup> value of 0.28 at the summit contour, Fig. 3c), suggesting that  
 327 this morphologic trend is a direct consequence of the conical nature of volcanoes. Furthermore, non-normalized  
 328 summit basin numbers also demonstrate a weak temporal trend, both at the upper 30% height designation (Fig. 7b)  
 329 as well as other percentages (Fig. S6). This suggests that basins that initially form on the summit region may retain  
 330 their topographic position as the edifice erodes. However, Fig. 3f demonstrates that these basins still widen through



331 time, to a width angle of  $\sim 60^\circ$  (though further analysis on older volcanoes is needed to explore whether this persists  
 332 on the Myr-timescale).



333  
 334 **Figure 7 – a:** Normalized number of basins along normalized relief for each volcano; colors are log-mean edifice age. **b:**  
 335 **Non-normalized number of summit basins** (defined by the upper 30% of the edifice’s height; black-dashed line of a)  
 336 compared to log-mean edifice age. **c:** Average along-perimeter summit basin distance compared to edifice age. **d:** Summit  
 337 basin spacing ratio (data from Fig. 4b divided by data from c) compared to edifice age. Colors and symbols in b-d are the  
 338 same as Fig. 3.

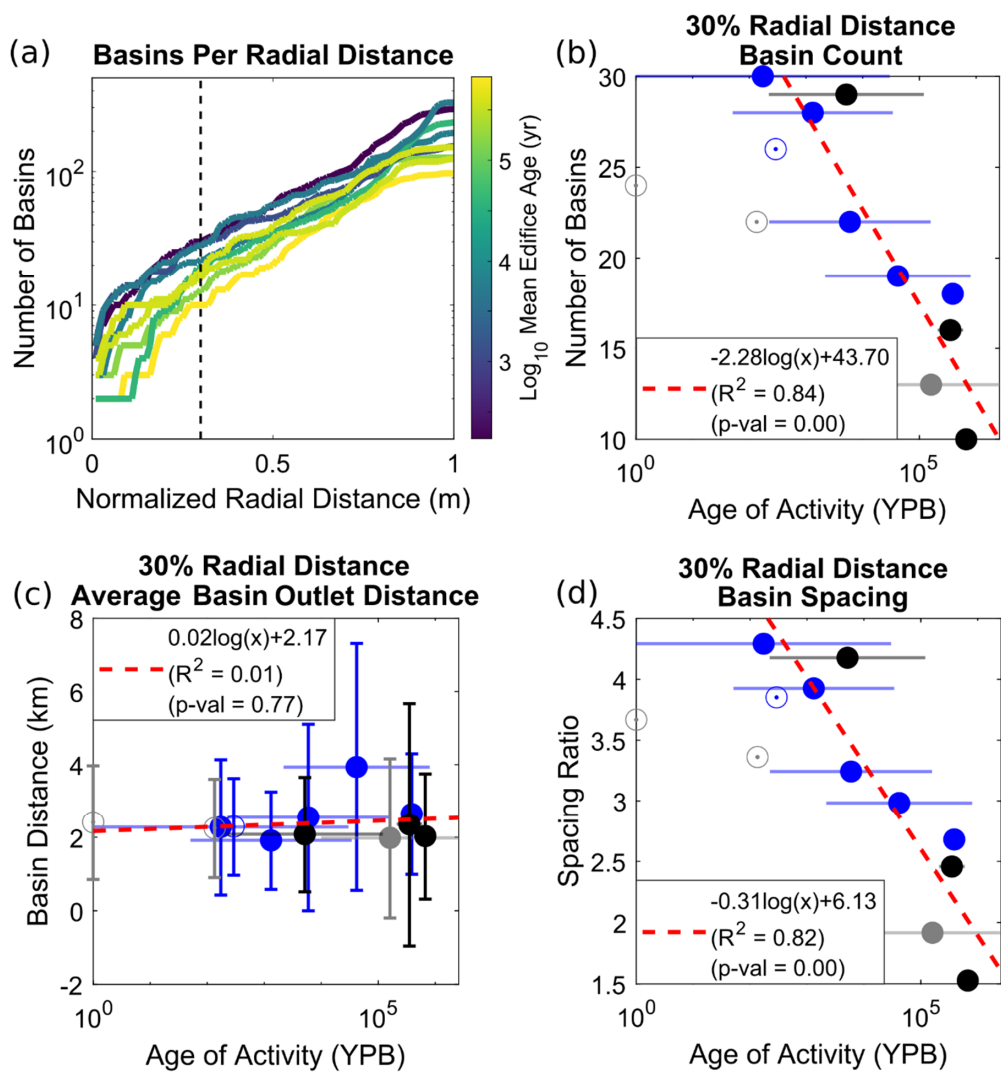
339 An apparent contradiction occurs when comparing mean summit basin width angles to the number of summit basins.  
 340 If all summit basins reached a width angle of  $\sim 60^\circ$ , it would be expected that only  $\sim 6$  basins would exist at the  
 341 summit; however, Fig. 7b shows that the number of basins that reach the summit on all edifices is greater than 10.  
 342 This difference is a consequence of how basin widths are calculated – by normalizing basin widths as an angle



343 relative to the distance from the summit to the widest part of the basin, basins become normalized by different  
344 lengths corresponding to their widest regions. Indeed, as discussed in Section 5.2, divide asymmetry is most  
345 frequent in the mid- and lower-flanks of the edifice (Fig. 6), thus accommodating largest basin widths at different  
346 sections of the flank.

347 If the number of basins that reach the summit is time invariant, how does this translate to the circumferential spacing  
348 of their outlets at the base of the edifice? Hovius (1996) compiled the ratio between mountain belt half-widths  
349 (distance between the major divide and mountain front,  $W_M$ ) and distances between major drainage basin outlets  
350 (those that reach the major divide;  $s$ ) in 11 mountain ranges globally, and determined a globally-averaged spacing  
351 ratio ( $W_M / s$ ) of  $\sim 2$ -3. We perform a similar analysis by dividing edifice effective radii by the average along-  
352 perimeter spacing between summit basin outlets. Figs 4b and 7c shows that while edifice effective radii decrease  
353 through time, so does the average perimeter distance between summit basin outlets. These behaviors thus combine  
354 to produce a relatively constant summit basin spacing ratio  $\sim 1.8 - 3.1$  (Fig. 7d), consistent with Hovius (1996) as  
355 well as modeling studies of drainage patterns (Habousha et al., 2023). This suggests that while summit basins  
356 azimuthally expand their widths, the edifice is also decreasing in area as the landform erodes, thus decreasing the  
357 distances between summit basin outlets.

358 However, a different behavior emerges when considering basins by their radial distance relative to the edifice's peak  
359 (Fig. 8), which is more sensitive to the areal expansion of basins along the edifice's flank. Plotting the non-  
360 normalized number of basins as a function of radial distance (normalized by maximum radius for each edifice) and  
361 time shows a clear temporal trend (Fig. 8a), with younger edifices having more basins along all sections of the  
362 volcano (as schematized in Fig. 5). This trend becomes more apparent through the logarithmic regression between  
363 log-mean edifice age and the number of basins that exist at 30% radial distance from the peak (Fig. 8b), and at other  
364 normalized distances (Fig. S7). Conducting a similar outlet perimeter-distance analysis on these basins shows that  
365 the average distance between basin outlets is relatively constant at  $\sim 2$  km (Fig. 8c), giving a strong ( $R^2 = 0.82$ )  
366 temporal decrease in basin spacing ratios (Fig. 8d). This behavior is similar to that described for the evolution of  
367 basin spacing on linear fault blocks (Talling et al., 1997) and is associated with the decreasing number of basins  
368 through time (driven by basin widening), highlighting the evolution and dynamics of radial drainage basins on  
369 volcanic edifices.



370

371 **Figure 8 – a:** Non-normalized number of basins as a function of normalized distance from the edifice’s peak; colors are  
 372 log-mean edifice age, black-dashed line represents 30% normalized distance from the edifice’s peak. **b:** Non-normalized  
 373 number of basins within 30% of the edifice’s peak (black-dashed line of a) compared to log-mean edifice age. **c:** Average  
 374 along-perimeter basin distance compared to edifice age. **d:** Basin spacing ratio (data from Fig. 4b divided by data from Fig. 3)  
 375 compared to edifice age. Colors and symbols in b-d are the same as Fig. 3.

376 **4.4 Radial drainage basin area-length relationship**

377 As a final observation for volcanic edifice drainage basins, we consider basin geometries in reference to Hack’s  
 378 power-law relationships between basin areas and lengths (Hack, 1957). Our analysis indicates that basins with  
 379 drainage areas greater than  $10^5 \text{ m}^2$  are well-fit by a power-law regression (Figs. 2b, 9a, c), whereas basins smaller  
 380 than  $10^5 \text{ m}^2$  have steeper trends between basin area and length, and are likely non-fluvial within the bounds of the  
 381 edifice.



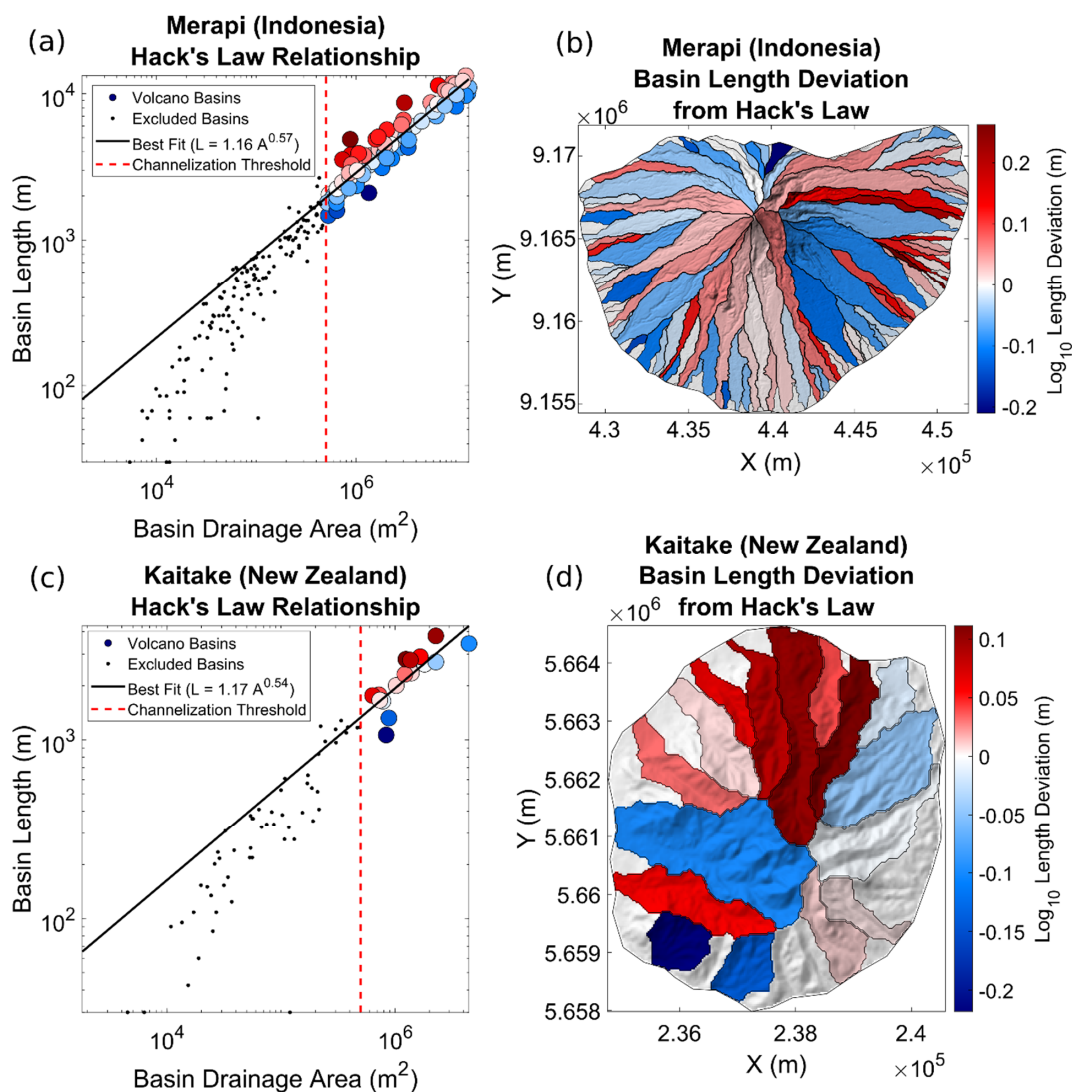
382 Analyzing Hack's Law regressions for Merapi and Kaitake (Fig. 9), the relationships between spatial location and  
383 basin geometries become apparent. Basins that are less than  $10^5 \text{ m}^2$  are constrained to the lowest regions of the  
384 edifice's flank, likely corresponding to non-channeled surfaces. Of those considered for the Hack's Law regression,  
385 the  $\log_{10}$  basin length deviation ( $D_L$ ) from the power-law is calculated as

$$386 \quad D_L = \log_{10}(L_H(A)) - \log_{10}(L), \quad (9)$$

387 where  $L_H$  is the basin length of the Hack's Law regression from a given basin's area ( $A$ ), and  $L$  is the basin's length.  
388 As expected from the geometric relationship, basins that fall below the power-law regression ( $D_L < 0$ ) are wider,  
389 and those that are above the power-law regression ( $D_L > 0$ ) are narrower.

390 Calculating  $D_L$  for basins with areas greater than our imposed channelization threshold ( $0.5 \text{ km}^2$ ), we do not observe  
391 any specific spatial pattern related to basins that deviate above or below the Hack's Law regression. However, one  
392 clear observation is the presence of highly-elongated basins on Merapi that exist on the mid- to upper-flanks and  
393 have  $D_L$  values  $> 0.2$  (Fig. 9b). These basins appear wedged or pinched between larger basins and would be  
394 expected to not have as much growth potential compared to their wider neighbors. Elongated basins also exist on  
395 Kaitake; however, they do not have as high of a deviation (maximum  $D_L \approx 0.1$ ; Fig. 9d). This may be a product of  
396 the lower number of basins that exist on Kaitake, or the overall lower amount of drainage area that Kaitake basins  
397 occupy, decreasing the amount of variability from the power law relationship. On both Merapi and Kaitake, these  
398 elongated basins may further highlight the dynamics of basin competition on radial structures – through drainage  
399 divide migration and areal loss (likely influenced by edifice-scale sector collapses or regrowth events; Gertisser et  
400 al., 2023), less-erosive and lower-order drainages become passive players to more dominant basins and adopt non-  
401 standard geometries, becoming narrow, chute-like basins on the mid- and upper-flanks. The generation of these  
402 narrow, 'nested' basins has also been observed to occur in response to differential tectonic uplift within analog and  
403 numerical experiments (Habousha et al., 2023).





404

405 **Figure 9 – Hack's Law analysis of (a-b) Merapi and (c-d) Kaitake. a, c: Basin drainage area – length relationships. Black**  
 406 **lines represent Hack's Law regressions. Colored circles correspond to the deviation from the regression trend (eq. 9),**  
 407 **associated with the color bars in b and d. Red-dashed line is imposed 0.5 km<sup>2</sup> channelization threshold, black dots are**  
 408 **basins less than the threshold and excluded from the regression. b, d: Maps showing the deviation of each basin from the**  
 409 **best-fit power-law regression.**

410 **4.5 How do radial drainages compare to other settings?**

411 Thus far, our discussion has focused on deriving a foundational understanding of how radial drainages on volcanic  
 412 edifices evolve and compete. However, we note similarities between our interpretation and those from previous  
 413 studies in other drainage settings. This leads to a simple question – is there a significant difference between radial  
 414 and dendritic drainage development and evolution?



415 Our results show that basin formation on edifices follows the development of rills and gullies within badlands  
416 (Schumm, 1956). As radial drainages evolve and certain basins expand to become dominant features on the edifice,  
417 less-dominant basins become passive and are pushed down-flank as nested basins, often adhering to non-standard  
418 geometries as imposed by their more-dominant neighbors (Habousha et al., 2023; Beeson and McCoy, 2022). The  
419 dynamics of this basin competition and formation of nested basins is demonstrated by edifice basin spacing ratios.  
420 Summit basins on edifices have spacing ratios that appear time-independent and fit within the range of values  
421 observed in linear mountain ranges globally (Hovius, 1996) (Fig. 7), suggesting the spacing of these basins is set  
422 during the initial stages of basin formation – an attribute of basin evolution that has been shown to occur on linear  
423 fault blocks (Talling et al., 1997; Habousha et al., 2023); however, basins that are within a radial distance from the  
424 summit that is 30% of the edifice’s maximum radius do experience a temporally-decreasing spacing ratio and  
425 constant distance between outlets (Fig. 8), capturing the development of a basin topographic hierarchy along the  
426 edifice – a behavior not previously observed. Finally, our drainage divide analysis on volcanic edifices suggest that  
427 radial drainage basins evolve towards a stable basin configuration as topography matures towards a dynamic  
428 equilibrium, similar to regional landscape evolution globally (e.g., Perron and Royden, 2013; Willett et al., 2014).

429 This comparison suggests that drainage development and evolution on radial structures are largely similar to those  
430 occurring within linear mountain settings. However, some differences still occur, particularly in relation to basin  
431 geometries imposed by the larger-scale, radial primary landform. Dendritic drainages in linear mountain belts and  
432 fault blocks are characterized by their leaf-like geometries (e.g., Zernitz, 1932; Strahler, 1952; Talling et al., 1997),  
433 having a broad headwater region that decreases towards the outlet to a tapered point. Although radial drainages also  
434 have tapered outlets and basin widths increase upstream, these widths are hindered by the conical geometry of the  
435 primary landform and convergence of multiple basins towards the summit, leading to a tapered headwater as well as  
436 a tapered outlet. This geometric constraint is well-demonstrated by the drainages on Merapi (Fig. 9b), where summit  
437 basins are generally widest on the lower- or mid-flanks; however, this trend is not as obvious on Kaitake (Fig. 9d),  
438 where erosion has dissected the landform and weakened the conical influence of the edifice on basin geometries.  
439 Furthermore, as edifice drainages are limited to an isolated, conical landform, their evolution and configuration are  
440 constrained by a cumulative areal limit. As opposed to linear mountain ranges (where a morphologic change in one  
441 basin impacts its neighbors, which then impacts their neighbors as a cascading chain across the landscape), on  
442 volcanic edifices, a morphologic change in one basin (particularly a dominant basin) may directly impact the  
443 erosional state and morphology of most other basins on the landform due to the high number of basins that may  
444 share a divide with this basin. This areal effect on radial basin evolution may be further augmented by the higher  
445 diversity of underlying host rocks between edifice basins associated with magmatic and volcanic products (e.g.,  
446 tephra deposits, lava flows, intrusions) that is not as prevalent within linear mountain ranges.

447 Despite the differences in basin geometries and interactions discussed above, edifice-averaged morphometric values  
448 (e.g., Hack’s Law exponent, drainage density, mean basin hypsometry, mean basin slopes) are similar to those of  
449 other settings (Hack, 1957; Strahler, 1952; Horton, 1945). This suggests that although radial drainages experience  
450 phenomena that differ from those typically experienced in dendritic settings, drainage development, geometries, and



451 competition largely follow those of dendritic patterns. As volcanic surfaces are easily datable and their ages can  
452 often vary by orders magnitude on a single edifice, volcanoes represent ideal locations for studying terrain evolution  
453 over varying temporal scales within a general framework.

#### 454 **4.6 Basin morphology capturing volcanic processes**

455 In this study, we considered edifice morphologies using mean values over the entire edifice. However, our metrics  
456 also allow for the comparison of basin morphologies on a single edifice. Variations associated with these metrics  
457 would likely relate to spatially-localized attributes of aggradation, degradation, and climate, and would thus provide  
458 a quantitative method to disentangle these signals using topography. For example, edifice flanks that have been  
459 resurfaced by large volcanic deposits or destroyed by sector collapses should exhibit younger drainage networks  
460 according to the metrics explored here that differ from other parts of the volcano. Furthermore, alterations to the  
461 erosional efficiency of a basin by tephra accumulation or lava flow emplacement should create spatial variability  
462 that can be quantified by similar analyses. These concepts should be tested over well-constrained cases and would  
463 be beneficial for both preliminary fieldwork and to approximate relative volcanic chronologies remotely. Our model  
464 for edifice degradation, radial drainage evolution, and divide stability thus provides a first step to deconvolving the  
465 various signals that relate to edifice morphology. This presents new avenues of exploration for the volcanology  
466 community to interrogate volcanic histories from topography, and for the geomorphic community to investigate  
467 surface evolution on landforms that often fall outside standard tectonic studies.

#### 468 **5.0 Conclusion**

469 Volcanic edifices represent a class of primary landforms whose erosion remains relatively unexplored. We analyzed  
470 the degradational histories of volcanic edifices using a set of metrics that have not previously been considered for  
471 radial drainage networks. We show that these metrics relate to the overall age of a volcano and propose a new  
472 general model for the temporal evolution of edifice drainage morphology. Divide stability analysis underscores the  
473 dynamic nature of basin evolution, and suggests radial drainage networks initiate with nearly-uniform geometries  
474 and unstable configurations that evolve towards non-uniform basin geometries and more stable configurations to  
475 generate a basin topographic hierarchy on volcanoes. Finally, comparing basin geometries, configurations, and  
476 outlet spacing between basins that exist on volcanic edifices to those that exist on linear mountain ranges highlights  
477 similarities and differences between radial and dendritic drainage basins.

#### 478 **6.0 Code availability**

479 DrainageVolc and MorVolc codes are available at [https://github.com/danjohara/Volc\\_Packages](https://github.com/danjohara/Volc_Packages).

#### 480 **7.0 Data availability**

481 Collected edifice data is included in the supplement as both an Excel file and shapefile.

#### 482 **8.0 Author contribution**

483 All authors provided editorial advice on the manuscript. DO'H wrote the DrainageVolc and updated MorVolc codes,  
484 conducted the morphology analyses, and wrote the manuscript. RMJvW assisted in data collection, determined  
485 edifice boundaries from topography, and tested DrainageVolc/MorVolc. LG and BC gave advice on drainage basin  
486 morphology and evolution, while PG, PL, and GK provided insight on volcanic edifice morphology, evolution, and



487 general volcano ages. MK secured funds and coordinated the project, giving advice on the research direction,  
488 analyses, and interpretation.

#### 489 **9.0 Competing interests**

490 The authors declare that they have no conflict of interest.

#### 491 **10.0 Acknowledgement**

492 This research was funded through the EVoLvE project, Junior FWO project grant G029820N of the Fonds  
493 Wetenschappelijke Onderzoek – Vlaanderen.

#### 494 **11.0 References**

- 495 Becerril, L., Lara, L. E., and Astudillo, V. I.: The strong competition between growth and erosive processes on the  
496 Juan Fernández Archipelago (SE Pacific, Chile), *Geomorphology*, 373, 107513,  
497 <https://doi.org/10.1016/j.geomorph.2020.107513>, 2021.
- 498 Beeson, H. W. and McCoy: Disequilibrium river networks dissecting the western slope of the Sierra Nevada,  
499 California, USA, record significant late Cenozoic tilting and associated surface uplift, *Bull. Geol. Soc. Am.*, 134,  
500 2809–2853, <https://doi.org/10.1130/B36517.1>, 2022.
- 501 Biggs, J., Mothes, P., Ruiz, M., Amelung, F., Dixon, T. H., Baker, S., and Hong, S. H.: Stratovolcano growth by co-  
502 eruptive intrusion: The 2008 eruption of Tungurahua Ecuador, *Geophys. Res. Lett.*, 37,  
503 <https://doi.org/10.1029/2010GL044942>, 2010.
- 504 Bishop, P.: Drainage rearrangement by river capture, beheading and diversion, *Prog. Phys. Geogr.*, 19, 449–473,  
505 1995.
- 506 Bohnenstiehl, D. W. R., Howell, J. K., White, S. M., and Hey, R. N.: A modified basal outlining algorithm for  
507 identifying topographic highs from gridded elevation data, Part 1: Motivation and methods, *Comput. Geosci.*, 49,  
508 308–314, <https://doi.org/10.1016/j.cageo.2012.04.024>, 2012.
- 509 Braun, J.: A review of numerical modeling studies of passive margin escarpments leading to a new analytical  
510 expression for the rate of escarpment migration velocity, *Gondwana Res.*, 53, 209–224,  
511 <https://doi.org/10.1016/j.gr.2017.04.012>, 2018.
- 512 Castellort, S. and Simpson, G.: River spacing and drainage network growth in widening mountain ranges, *Basin*  
513 *Res.*, 18, 267–276, <https://doi.org/10.1111/j.1365-2117.2006.00293.x>, 2006.
- 514 Castellort, S., Simpson, G., and Darrioulat, A.: Slope-control on the aspect ratio of river basins, *Terra Nov.*, 21,  
515 265–270, <https://doi.org/10.1111/j.1365-3121.2009.00880.x>, 2009.
- 516 Castellort, S., Goren, L., Willett, S. D., Champagnac, J. D., Herman, F., and Braun, J.: River drainage patterns in  
517 the New Zealand Alps primarily controlled by plate tectonic strain, *Nat. Geosci.*, 5, 744–748,  
518 <https://doi.org/10.1038/ngeo1582>, 2012.
- 519 Castro, J. M., Cordonnier, B., Schipper, C. I., Tuffen, H., Baumann, T. S., and Feisel, Y.: Rapid laccolith intrusion  
520 driven by explosive volcanic eruption, *Nat. Commun.*, 7, 1–7, <https://doi.org/10.1038/ncomms13585>, 2016.
- 521 Civico, R., Ricci, T., Scarlato, P., Taddeucci, J., Andronico, D., Del Bello, E., D’Auria, L., Hernández, P. A., and  
522 Pérez, N. M.: High-resolution Digital Surface Model of the 2021 eruption deposit of Cumbre Vieja volcano, La  
523 Palma, Spain, *Sci. Data*, 9, 1–7, <https://doi.org/10.1038/s41597-022-01551-8>, 2022.
- 524 Cook, K. L., Turowski, J. M., and Hovius, N.: A demonstration of the importance of bedload transport for fluvial  
525 bedrock erosion and knickpoint propagation, *Earth Surf. Process. Landforms*, 38, 683–695,  
526 <https://doi.org/10.1002/esp.3313>, 2013.
- 527 Duvall, A. R. and Tucker, G. E.: Dynamic Ridges and Valleys in a Strike-Slip Environment, *J. Geophys. Res. F*  
528 *Earth Surf.*, 120, 2016–2026, <https://doi.org/10.1002/2015JF003618>, 2015.



- 529 Euillades, L. D., Grosse, P., and Euillades, P. A.: NETVOLC: An algorithm for automatic delimitation of volcano  
530 edifice boundaries using DEMs, *Comput. Geosci.*, 56, 151–160, <https://doi.org/10.1016/j.cageo.2013.03.011>, 2013.
- 531 Farr, T. G., Rosen, P. A., Caro, E., Crippen, R., Duren, R., Hensley, S., Kobrick, M., Paller, M., Rodriguez, E.,  
532 Roth, L., Seal, D., Shaffer, S., Shimada, J., Umland, J., Werner, M., Oskin, M., Burbank, D., and Alsdorf, D.: The  
533 Shuttle Radar Topography Mission, *Rev. Geophys.*, 45, 1–43, 2007.
- 534 Ferrier, K. L., Huppert, K. L., and Perron, J. T.: Climatic control of bedrock river incision, *Nature*, 496, 206–209,  
535 <https://doi.org/10.1038/nature11982>, 2013.
- 536 Flint, J. J.: Stream gradient as a function of order, magnitude, and discharge, *Water Resour. Res.*, 10, 969–973,  
537 <https://doi.org/10.1029/WR010i005p00969>, 1974.
- 538 Forte, A. M. and Whipple, K. X.: Criteria and tools for determining drainage divide stability, *Earth Planet. Sci. Lett.*,  
539 493, 102–117, <https://doi.org/10.1016/j.epsl.2018.04.026>, 2018.
- 540 Fox, M., Goren, L., May, D. A., and Willett, S. D.: Inversion of fluvial channels for paleorock uplift rates in Taiwan,  
541 *J. Geophys. Res. Earth Surf.*, 119, 1853–1875, <https://doi.org/10.1002/2014JF003196>, 2014.
- 542 Gase, A. C., Brand, B. D., and Bradford, J. H.: Evidence of erosional self-channelization of pyroclastic density  
543 currents revealed by ground-penetrating radar imaging at Mount St. Helens, Washington (USA), *Geophys. Res.*  
544 *Lett.*, 44, 2220–2228, <https://doi.org/10.1002/2016GL072178>, 2017.
- 545 Gertisser, R., Troll, V. R., Walter, T. R., Nandaka, I. G. M. A., and Ratdompurbo, A.: Merapi Volcano: Geology,  
546 Eruptive Activity, and Monitoring of a High-Risk Volcano, Springer Nature, 2023.
- 547 Gilbert, G. K.: The Convexity of Hilltops, *J. Geol.*, 17, 344–350, 1909.
- 548 Grosse, P., van Wyk de Vries, B., Petrinovic, I. A., Euillades, P. A., and Alvarado, G. E.: Morphometry and  
549 evolution of arc volcanoes, *Geology*, 37, 651–654, <https://doi.org/10.1130/G25734A.1>, 2009.
- 550 Grosse, P., van Wyk de Vries, B., Euillades, P. A., Kervyn, M., and Petrinovic, I. A.: Systematic morphometric  
551 characterization of volcanic edifices using digital elevation models, *Geomorphology*, 136, 114–131,  
552 <https://doi.org/10.1016/j.geomorph.2011.06.001>, 2012.
- 553 Habousha, K., Goren, L., Nativ, R., and Gruber, C.: Plan-Form Evolution of Drainage Basins in Response to  
554 Tectonic Changes: Insights From Experimental and Numerical Landscapes, *J. Geophys. Res. Earth Surf.*, 128, 1–24,  
555 <https://doi.org/10.1029/2022jf006876>, 2023.
- 556 Hack, J. T.: Studies of longitudinal stream profiles in Virginia and Maryland, USGS Prof. Pap. 249, 97, 1957.
- 557 Hamawi, M., Goren, L., Mushkin, A., and Levi, T.: Rectangular drainage pattern evolution controlled by pipe cave  
558 collapse along clastic dikes, the Dead Sea Basin, Israel, *Earth Surf. Process. Landforms*, 47, 936–954,  
559 <https://doi.org/10.1002/esp.5295>, 2022.
- 560 Han, J., Gasparini, N. M., and Johnson, J. P. L.: Measuring the imprint of orographic rainfall gradients on the  
561 morphology of steady-state numerical fluvial landscapes, *Earth Surf. Process. Landforms*, 40, 1334–1350,  
562 <https://doi.org/10.1002/esp.3723>, 2015.
- 563 Hasbargen, L. E. and Paola, C.: Landscape instability in an experimental drainage basin, *Geology*, 28, 1067–1070,  
564 [https://doi.org/10.1130/0091-7613\(2000\)28<1067:LIIAED>2.0.CO;2](https://doi.org/10.1130/0091-7613(2000)28<1067:LIIAED>2.0.CO;2), 2000.
- 565 Hayes, S. K., Montgomery, D. R., and Newhall, C. G.: Fluvial sediment transport and deposition following the 1991  
566 eruption of Mount Pinatubo, *Geomorphology*, 45, 211–224, [https://doi.org/10.1016/S0169-555X\(01\)00155-6](https://doi.org/10.1016/S0169-555X(01)00155-6), 2002.
- 567 Horton, R. E.: Erosional development of streams and their drainage basins; hydrological approach to quantitative  
568 morphology, *Geol. Soc. Am. Bull.*, 56, 275–370, [https://doi.org/10.1130/0016-7606\(1945\)56\[275:EDOSAT\]2.0.CO;2](https://doi.org/10.1130/0016-7606(1945)56[275:EDOSAT]2.0.CO;2), 1945.
- 570 Hovius, N.: Regular spacing of drainage outlets from linear mountain belts, *Basin Res.*, 8, 29–44,  
571 <https://doi.org/10.1111/j.1365-2117.1996.tb00113.x>, 1996.



- 572 Howard, A. D.: Drainage Analysis in Geologic Interpretation: A Summation, *Am. Assoc. Pet. Geol. Bull.*, 51,  
573 <https://doi.org/10.1306/5d25c26d-16c1-11d7-8645000102c1865d>, 1967.
- 574 Jefferson, A., Grant, G. E., Lewis, S. L., and Lancaster, S. T.: Coevolution of hydrology and topography on a basalt  
575 landscape in the Oregon Cascade Range, USA, *Earth Surf. Process. Landforms*, 35, 803–816,  
576 <https://doi.org/10.1002/esp.1976>, 2010.
- 577 Karátson, D., Thouret, J. C., Moriya, I., and Lomoschitz, A.: Erosion calderas: Origins, processes, structural and  
578 climatic control, *Bull. Volcanol.*, 61, 174–193, <https://doi.org/10.1007/s004450050270>, 1999.
- 579 Karátson, D., Telbisz, T., and Wörner, G.: Erosion rates and erosion patterns of Neogene to Quaternary  
580 stratovolcanoes in the Western Cordillera of the Central Andes: An SRTM DEM based analysis, *Geomorphology*,  
581 139–140, 122–135, <https://doi.org/10.1016/j.geomorph.2011.10.010>, 2012.
- 582 Kerr, R. C.: Thermal erosion by laminar lava flows, *J. Geophys. Res. B Solid Earth*, 106, 453–465,  
583 <https://doi.org/10.1029/2001JB000227>, 2001.
- 584 Kirby, E. and Whipple, K. X.: Expression of active tectonics in erosional landscapes, *J. Struct. Geol.*, 44, 54–75,  
585 <https://doi.org/10.1016/j.jsg.2012.07.009>, 2012.
- 586 Kirby, E., Whipple, K. X., Tang, W., and Chen, Z.: Distribution of active rock uplift along the eastern margin of the  
587 Tibetan Plateau: Inferences from bedrock channel longitudinal profiles, *J. Geophys. Res. Solid Earth*, 108,  
588 <https://doi.org/10.1029/2001JB000861>, 2003.
- 589 Lahitte, P., Samper, A., and Quidelleur, X.: DEM-based reconstruction of southern Basse-Terre volcanoes  
590 (Guadeloupe archipelago, FWI): Contribution to the Lesser Antilles Arc construction rates and magma production,  
591 *Geomorphology*, 136, 148–164, <https://doi.org/10.1016/j.geomorph.2011.04.008>, 2012.
- 592 Lohse, K. A. and Dietrich, W. E.: Contrasting effects of soil development on hydrological properties and flow paths,  
593 41, <https://doi.org/10.1029/2004WR003403>, 2005.
- 594 Mejía, A. I. and Niemann, J. D.: Identification and characterization of dendritic, parallel, pinnate, rectangular, and  
595 trellis networks based on deviations from planform self-similarity, *J. Geophys. Res. Earth Surf.*, 113, 1–21,  
596 <https://doi.org/10.1029/2007JF000781>, 2008.
- 597 Montgomery, D. R. and Dietrich, W. E.: Landscape Dissection and Drainage Area-Slope Threshold, in: *Process  
598 Models and Theoretical Geomorphology*, 1, 1994.
- 599 Mudd, S. M. and Furbish, D. J.: Responses of soil-mantled hillslopes to transient channel incision rates, *J. Geophys.  
600 Res. Earth Surf.*, 112, 1–12, <https://doi.org/10.1029/2006JF000516>, 2007.
- 601 Mueller, J. E.: Re-evaluation of the relationship of master streams and drainage basins, *Bull. Geol. Soc. Am.*, 83,  
602 3471–3474, [https://doi.org/10.1130/0016-7606\(1972\)83\[3471:ROTR0M\]2.0.CO;2](https://doi.org/10.1130/0016-7606(1972)83[3471:ROTR0M]2.0.CO;2), 1972.
- 603 O’Hara, D. and Karlstrom, L.: The arc-scale spatial distribution of volcano erosion implies coupled magmatism and  
604 regional climate in the Cascades arc, United States, *Front. Earth Sci.*, 11, 1–15,  
605 <https://doi.org/10.3389/feart.2023.1150760>, 2023.
- 606 O’Hara, D., Karlstrom, L., and Roering, J. J.: Distributed landscape response to localized uplift and the fragility of  
607 steady states, *Earth Planet. Sci. Lett.*, 506, 243–254, <https://doi.org/10.1016/j.epsl.2018.11.006>, 2019.
- 608 O’Hara, D., Karlstrom, L., and Ramsey, D. W.: Time-evolving surface and subsurface signatures of Quaternary  
609 volcanism in the Cascades arc, *Geology*, 49, e526, <https://doi.org/10.1130/g47706.1>, 2020.
- 610 Ollier, C.: *Volcanoes*, edited by: Blackwell, B., Oxford:, 288 pp., 1988.
- 611 Perron, J. T. and Royden, L.: An integral approach to bedrock river profile analysis, *Earth Surf. Process. Landforms*,  
612 38, 570–576, <https://doi.org/10.1002/esp.3302>, 2013.
- 613 Pierson, T. C. and Major, J. J.: Hydrogeomorphic effects of explosive volcanic eruptions on drainage basins, *Annu.  
614 Rev. Earth Planet. Sci.*, 42, 469–507, <https://doi.org/10.1146/annurev-earth-060313-054913>, 2014.



- 615 Prince, P. S. and Spotila, J. A.: Evidence of transient topographic disequilibrium in a landward passive margin river  
616 system: Knickpoints and paleo-landscapes of the New River basin, southern Appalachians, *Earth Surf. Process.*  
617 *Landforms*, 38, 1685–1699, <https://doi.org/10.1002/esp.3406>, 2013.
- 618 Ricci, J., Lahitte, P., Quidelleur, X., Ricci, J., Lahitte, P., and Quidelleur, X.: Construction and destruction rates of  
619 volcanoes within tropical environment: Examples from the Basse-Terre Island (Guadeloupe, Lesser Antilles),  
620 *Geomorphology*, 228, 597–607, <https://doi.org/10.1016/j.geomorph.2014.10.002>, 2015.
- 621 Scherler, D. and Schwanghart, W.: Drainage divide networks - Part 1: Identification and ordering in digital elevation  
622 models, *Earth Surf. Dyn.*, 8, 245–259, <https://doi.org/10.5194/esurf-8-245-2020>, 2020.
- 623 Schumm, S. A.: Evolution of drainage systems and slopes in badlands at Perth Amboy, New Jersey, *Bull. Geol. Soc.*  
624 *Am.*, 67, 597–646, [https://doi.org/10.1130/0016-7606\(1956\)67\[597:EODSAS\]2.0.CO;2](https://doi.org/10.1130/0016-7606(1956)67[597:EODSAS]2.0.CO;2), 1956.
- 625 Schwanghart, W. and Scherler, D.: Short Communication: TopoToolbox 2 - MATLAB-based software for  
626 topographic analysis and modeling in Earth surface sciences, *Earth Surf. Dyn.*, 2, 1–7, [https://doi.org/10.5194/esurf-](https://doi.org/10.5194/esurf-2-1-2014)  
627 [2-1-2014](https://doi.org/10.5194/esurf-2-1-2014), 2014.
- 628 Shea, T. and van Wyk de Vries, B.: Structural analysis and analogue modeling of the kinematics and dynamics of  
629 rockslide avalanches, *Geosphere*, 4, 657–686, <https://doi.org/10.1130/GES00131.1>, 2008.
- 630 Sklar, L. S. and Dietrich, W. E.: Sediment and rock strength controls on river incision into bedrock, *Geology*, 29,  
631 1087–1090, [https://doi.org/10.1130/0091-7613\(2001\)029<1087:SARSCO>2.0.CO;2](https://doi.org/10.1130/0091-7613(2001)029<1087:SARSCO>2.0.CO;2), 2001.
- 632 Strahler, A. N.: Hypsometric (area-altitude) analysis of erosional topography, *Bull. Geol. Soc. Am.*, 63, 1117–1142,  
633 <https://doi.org/10.1128/AAC.03728-14>, 1952.
- 634 Sweeney, K. E. and Roering, J. J.: Rapid fluvial incision of a late Holocene lava flow: Insights from LiDAR, alluvial  
635 stratigraphy, and numerical modeling, *Bull. Geol. Soc. Am.*, 129, 500–512, <https://doi.org/10.1130/B31537.1>, 2017.
- 636 Talling, P. J., Stewart, M. D., Stark, C. P., Gupta, S., and Vincent, S. J.: Regular spacing of drainage outlets from  
637 linear fault blocks, *Basin Res.*, 9, 275–302, <https://doi.org/10.1046/j.1365-2117.1997.00048.x>, 1997.
- 638 Thouret, J. C., Oehler, J. F., Gupta, A., Solikhin, A., and Procter, J. N.: Erosion and aggradation on persistently  
639 active volcanoes—a case study from Semeru Volcano, Indonesia, *Bull. Volcanol.*, 76,  
640 <https://doi.org/10.1007/s00445-014-0857-z>, 2014.
- 641 Ui, T. and Glicken, H.: Internal structural variations in a debris-avalanche deposit from ancestral Mount Shasta,  
642 California, USA, *Bull. Volcanol.*, 48, 189–194, <https://doi.org/10.1007/BF01087673>, 1986.
- 643 van Wees, R. M. J., Tournigand, P.-Y., O’Hara, D., Grosse, P., Kereszturi, G., Campforts, B., Lahitte, P., and  
644 Kervyn, M.: The role of erosion in the morphometry of composite volcanoes, in: EGU General Assembly  
645 Conference Abstracts, EGU21-14500, 2021.
- 646 Wells, S. G., Dohrenwend, J. C., McFadden, L. D., Turrin, B. D., and Mahrer, K. D.: Late Cenozoic landscape  
647 evolution on lava flow surfaces of the Cima volcanic field, Mojave Desert, California., *Geol. Soc. Am. Bull.*, 96,  
648 1518–1529, [https://doi.org/10.1130/0016-7606\(1985\)96<1518:LCLEOL>2.0.CO;2](https://doi.org/10.1130/0016-7606(1985)96<1518:LCLEOL>2.0.CO;2), 1985.
- 649 Whipple, K. X., DiBiase, R. A., Ouimet, W. B., and Forte, A. M.: Preservation or piracy: Diagnosing low-relief,  
650 high-elevation surface formation mechanisms, *Geology*, 45, 91–94, <https://doi.org/10.1130/G32501Y.1>, 2016.
- 651 Wicks, C. W., Dzurisin, D., Ingebritsen, S., Thatcher, W., Lu, Z., and Iverson, J.: Magmatic activity beneath the  
652 quiescent Three Sisters volcanic center, central Oregon Cascade Range, USA, *Geophys. Res. Lett.*, 29, 26-1-26–4,  
653 <https://doi.org/10.1029/2001GL014205>, 2002.
- 654 Willett, S. D., Slingerland, R., and Hovius, N.: Uplift, shortening, and steady state topography in active mountain  
655 belts, *Am. J. Sci.*, 301, 455–485, <https://doi.org/10.2475/ajs.301.4-5.455>, 2001.
- 656 Willett, S. D., McCoy, S. W., Perron, T. J., Goren, L., and Chen, C. Y.: Dynamic reorganization of River Basins,  
657 *Science (80-. )*, 343, <https://doi.org/10.1126/science.1248765>, 2014.



- 658 Yang, R., Willett, S. D., and Goren, L.: In situ low-relief landscape formation as a result of river network disruption,  
659 Nature, 520, 526–529, <https://doi.org/10.1038/nature14354>, 2015.
- 660 Zernitz, E. R.: Drainage Patterns and Their Significance, J. Geol., 40, 498–521, <https://doi.org/10.1086/623976>,  
661 1932.
- 662